

NACA RM E51G19



*C.F.*

# RESEARCH MEMORANDUM

EXPERIMENTAL INVESTIGATION OF A 16-INCH IMPULSE-TYPE  
SUPERSONIC-COMPRESSOR ROTOR

By Guy N. Ullman, Melvin J. Hartmann, and Edward R. Tysl

Lewis Flight Propulsion Laboratory  
Cleveland, Ohio

CLASSIFICATION CHANGED

UNCLASSIFIED

To \_\_\_\_\_

*NACA Re also*

By authority of *✓ RN-118* Date *effective July 26, 1957*

*AMT 8-21-57*

CLASSIFIED DOCUMENT

This document contains classified information affecting the National Defense of the United States within the meaning of the Espionage Act, USC 50:31 and 32. Its transmission or the revelation of its contents in any manner to an unauthorized person is prohibited by law.

Information so classified may be imparted only to persons in the military and naval services of the United States, appropriate civilian officers and employees of the Federal Government who have a legitimate interest therein, and to United States citizens of known loyalty and discretion who of necessity must be informed thereof.

## NATIONAL ADVISORY COMMITTEE FOR AERONAUTICS

WASHINGTON

October 5, 1951

NACA LIBRARY  
LANGLEY AERONAUTICAL RESEARCH CENTER  
RESEARCH REPORT



## NATIONAL ADVISORY COMMITTEE FOR AERONAUTICS

RESEARCH MEMORANDUMEXPERIMENTAL INVESTIGATION OF A 16-INCH IMPULSE-TYPE  
SUPERSONIC-COMPRESSOR ROTOR

By Guy N. Ullman, Melvin J. Hartmann, and Edward R. Tysl

## SUMMARY

Theoretical considerations of an impulse-type supersonic compressor in which the velocity relative to the rotor is supersonic indicate that good performance can be obtained with this type of compressor. In order to investigate this supersonic-compressor configuration, a 16-inch-diameter rotor was constructed and investigated in Freon-12. This rotor of moderate design turned the flow in the rotor approximately  $47^\circ$  and had relative entrance and exit Mach numbers approximately equal to 1.7. Data were obtained over a range of back pressures from 104 percent of design equivalent speed (design speed, 1604 ft/sec in air) to 55 percent of design equivalent speed in Freon-12. These data were converted to approximate equivalent-air results.

At 104 percent of design equivalent speed and impulse-type operation, this supersonic-compressor rotor produced a total-pressure ratio of 3.60, an adiabatic efficiency of 0.80, and an air equivalent mass flow of 29.1 pounds per second. Under these conditions the measured absolute exit Mach number (about 1.72) and absolute exit angle (about  $27^\circ$ ) were very near the design values. However, the rotor could also be operated with a high back pressure so that a compression shock was obtained in the rotor at about the same total-pressure ratio and equivalent weight flow, but with lower efficiency and absolute exit Mach number. The shock-in-rotor condition resulted in high absolute exit angles.

Operation was obtained with shock-free flow through the compressor rotor and the downstream annulus. Performance characteristics were continuous over the range of operation from open throttle to the stall point. A wide range of air equivalent weight flows was obtained at the reduced speeds; however, at higher speeds the weight flow was constant. This investigation indicates that stators downstream of this rotor must obtain the required diffusion without imposing a high back pressure on the compressor rotor.

## INTRODUCTION

In an effort to improve the total-pressure ratio per stage and at the same time obtain high unit weight flow ((lb/sec)/sq ft frontal area), several supersonic-compressor configurations are being investigated at the NACA Lewis laboratory. In reference 1, Kantrowitz points out that axial-flow supersonic compressors have these desirable characteristics and that they can be designed for efficient operation. He also indicates several possible configurations that might result in practical compressor stages. In reference 2, the velocity diagrams for four supersonic-compressor configurations are analyzed. The results of that investigation indicate that high pressure ratio and reasonably good characteristics might be obtained in an impulse-type supersonic compressor. In this type supersonic compressor, the energy input to the gas is achieved by supersonic turning in the compressor rotor; deceleration through the speed of sound is necessary in the exit stators. In reference 3, the results of cascade investigations of supersonic turning passages are used to determine the performance characteristics of this type supersonic compressor and some of the design problems are discussed.

Because of the favorable results of these analytical investigations, an investigation of impulse-type supersonic-compressors was initiated. The compressor rotor designed by the method described in the Apparatus section was of conservative design in order to facilitate the investigation of performance characteristics. The compressor rotor had an entrance outside diameter of 16 inches and an entrance hub-tip radius ratio of 0.75. The experimental-performance data reported herein for this impulse-type supersonic-compressor rotor with inlet guide vanes were obtained in Freon-12 (dichlorodifluoromethane), a commercial refrigerant.

## APPARATUS

Impulse-type supersonic-compressor rotor. - The impulse-type supersonic-compressor rotor used in this investigation is shown in figure 1. This compressor rotor was designed graphically by using a modified method of characteristics. Corrections to the two-dimensional characteristics when the disturbances occurred oblique to the flow were based on linearized flow theory. Developments that were made concurrently along several stream sheets resulted in a very tedious problem in descriptive geometry, which is not recommended as a general design procedure. The resulting blade contours and the hub and tip shapes are shown in figure 2.

The compressor rotor consisted of 29 blades and had a tip diameter of 16.0 inches, an entrance hub-tip radius ratio of 0.75, an exit hub-tip radius ratio of 0.867, and was about 4.0 inches deep. The inner and

outer shrouds were so contoured that the flow area (in the compressor rotor) at the rotor exit was essentially equal to that at the entrance with the mean radius remaining approximately constant. The design tip speed of the rotor was 1604 feet per second in air. Inlet guide vanes were used to establish a free-vortex flow opposite to the direction of rotation and the absolute flow angle varied from  $12^\circ$  at the tip to  $15^\circ$  at the hub. The resulting entrance Mach number relative to the blade at design speed was varied from 1.80 at the tip to 1.50 at the hub. The turning in the rotor passage was varied from  $40^\circ$  at the tip to  $52^\circ$  at the hub in an effort to equalize the energy input along the radius. This difference in rotor-passage turning resulted in an appreciable sweep at the trailing edge of the blade. The design (air) vector diagram for this rotor-tip section is shown in figure 3. (All symbols are defined in appendix A.)

Variable-component test rig. - The impulse-type supersonic-compressor rotor was installed in a variable-component test rig (fig. 4), which was adapted to use Freon-12 as the test medium. The compressor was driven by a 3000-horsepower variable-frequency motor through a speed increaser that allowed a maximum speed of 12,000 rpm. Because Freon-12 was used in these tests, the compressor discharge collector was connected to the entrance tank to form a recirculating system. In this system, the pressure developed by the compressor was dissipated across the cylindrical discharge throttle at the end of the radial diffuser. The hot gas flowed from the collector through twin cooler assemblies to the entrance tank. The rate of water flow through the coolers was varied to obtain the desired temperature in the entrance tank. The pressure level in the test loop was maintained at the desired point by controlling the amount of Freon-12 in the system. The purification system maintained a concentration of 97 percent or higher of Freon-12 by volume.

Instrumentation. - The over-all rating of the compressor was obtained as recommended in reference 4 by using the instrumentation in the entrance tank and that at station 5 (about 8.75 in. downstream of the rotor). Weight flow was measured by static pressures on the inlet fairing nozzle, which was calibrated against a known adjustable orifice. Inlet-stagnation conditions were measured in the entrance tank, which was 4 feet in diameter and 6 feet long. At station 5, two calibrated 3-point total-temperature rakes were used to measure exit temperature. Total-pressure probes (15) were arranged at area centers of three equal annular areas and were spaced at various circumferential locations to obtain an averaged downstream total pressure. Total-temperature and total-pressure instruments were set at an average angle as determined by tests and were insensitive to angle over the range of angles encountered.

At station 4, about  $3/4$  inch downstream of the rotor, a probe actuator was used to obtain surveys at various radial positions. The instrument used in this probe actuator (fig. 5) was a cone-type

combination instrument, which obtained total pressure at the tip of the cone and was calibrated to measure static pressure on the surface of the cone. The static pressure on opposite sides of the cone were used as a null-type angle-measuring device. At station 4, total pressures were measured by three total-pressure probes placed at the area centers of three equal annular areas.

Wall static pressures were obtained at each measuring station by means of the method recommended in reference 4. Static-pressure distributions were obtained by a series of wall static-pressure taps in the flow path.

Because it was necessary to maintain a Freon-12 purity of at least 0.97, a gas-density balance was used to measure the content of the test gas. For a part of the investigation, a second device that measured change in electric conductivity for the mixture was also used to determine the content of the test gas; results obtained with these two instruments were found to be equivalent.

#### PROCEDURE

Over-all performance data were obtained over a range of back pressures from open throttle to stall at six wheel speeds from 104 percent of design equivalent speed to about 55 percent of equivalent speed. For these data, the inlet stagnation pressure was maintained between 30 to 32 inches mercury absolute, and the inlet temperature was maintained between 100° and 130° F. Frequent measurements of the test-gas purity were made during the runs. Radial survey data were taken at station 4 for the design point. The discharge angle was measured at the pitch radius for all data points at which surveys were not obtained.

The compressor rotor was rated on conditions measured in the depression tank and station 5; thus the over-all performance data include the losses in the annulus between the rotor and the rake station. Total-pressure instruments in the supersonic stream were corrected for normal shock losses at the mean stream Mach number as determined by the wall static-pressure taps and the averaged total-pressure reading (see appendix B). All static-pressure survey probes and total-temperature probes were calibrated for the range of Mach numbers encountered.

#### ROTOR PERFORMANCE

The 16-inch impulse-type supersonic compressor was operated over a range of speeds and total-pressure ratios in Freon-12. The weight flow and the compressor speed were converted to approximate air equivalent results by the methods described in appendix B and the results of this experimental investigation are presented in the following section.

2247

Total-pressure ratio. - Total-pressure ratios  $P_5/P_1$  and air equivalent weight flows  $W\sqrt{\theta}/\delta$  obtained at several equivalent tip speeds from 55 to 104 percent of design equivalent tip speed are shown in figure 6. At 104, 97, and 91 percent of design equivalent tip speed, no appreciable variation in air equivalent weight flow occurs over the range of pressure ratios. At 83, 69, and 55 percent of design equivalent tip speed, there is a large range of air equivalent weight flows. At 69 and 55 percent of design equivalent tip speed, this variation is obtained at very nearly constant total-pressure ratio. The stall line rises at approximately a uniform rate with speed and approximate equivalent weight flow of air up to 97 percent of design equivalent speed. At this speed, the stall line curves up very sharply to reach the total-pressure ratio 3.60 at 104 percent of design equivalent speed.

Effect of back pressure at 104 percent of design equivalent speed. - In figure 7, the effects of back pressure are shown by a plot of the various parameters for the range of total-pressure ratios measured at station 5. Each of the conditions plotted has two values for each value of downstream total-pressure ratio. Each curve is marked to show the point representing the open-throttle condition. The portion of each curve labeled A-B represents impulse operation, whereas B-C represents shock-in-rotor operation. The leg of these curves, which represents impulse-type operation (A-B), results from changes in conditions in the annulus between the rotor and the downstream instrument station. In examining this portion of the operational range, it is found that at open throttle (A) the absolute Mach number at station 5 (fig. 7(a)) was 1.75 and approximately equal to the Mach number directly downstream of the compressor rotor at station 4 (fig. 7(b)). At this point supersonic flow results without shock through station 5. Because the instruments are all corrected for the supersonic Mach numbers, no shock losses are charged to the compressor-rotor performance and a high total-pressure ratio ( $P_5/P_1 = 3.60$ ) results. The open-throttle point represents impulse-type operation because the energy appears almost entirely in the form of kinetic energy. In impulse-type operation, the static pressure downstream of the rotor at station 4 is very close to the static pressure at the rotor entrance.

The changes that occur as the throttle is closed cause the total-pressure ratio to decrease to its minimum value (region A-B). As the back pressure is increased by closing the discharge throttle, a compression shock is moved upstream of the instrumentation at station 5. This compression shock results in losses that are no longer accounted for in the corrections to the instrument readings. As the throttle is closed from peak total-pressure ratio to minimum total-pressure ratio (A-B), the Mach number at station 5  $M_5$  continues to decrease from the open-throttle value of 1.73 to about 1.04 (fig. 7(a)). Because these changes in total-pressure ratio are a result of the shock losses in the

annulus downstream of the rotor, they do not affect the performance of the rotor or the conditions measured downstream of the rotor at station 4. Thus, the absolute exit Mach number at station 4 (fig. 7(b)) and its components (figs. 7(c) and 7(d)) remain constant. The Mach number relative to the compressor rotor (fig. 7(e)) remains at about 1.6 and the measured exit angle remains constant at  $27^\circ$  (fig. 7(f)). However, the adiabatic efficiency based on the downstream measurements of temperature and total pressure indicates a very large loss in adiabatic efficiency from a peak value of 0.80 at maximum total-pressure ratio to a value of 0.62 at minimum total-pressure ratio (fig. 7(g)).

The loss in total-pressure ratio is a result of the location of the instrument station; and if the data are recorded on an instrument directly downstream of the rotor, there is no change in the measurements until the compression shock has been moved between the instruments and the compressor rotor. Thus, if a compression shock can be moved between the compressor rotor and the instruments, the same changes (except the mixing losses) would result whatever the axial location of the instrument station.

In the region of minimum-pressure ratio (B), very rapid changes result in all conditions plotted in figure 6. At this point the compression shock has been moved up to the trailing edge of the compressor rotor, the compression shock is completely upstream of all instrumentation, and the lowest total-pressure ratio (2.805) and adiabatic efficiency (0.62) result. In this region (B), the high back pressure causes the compression shock to move into the rotor passage. The shock relative to the rotor results in a substantial drop in Mach number relative to the rotor ( $M'_4$ , fig. 7(d)). On examining the vector diagrams (fig. 8), it can be seen that this decrease in relative Mach number  $M'_4$  results in an increase in absolute exit tangential Mach number  $M_{\theta,4}$  and an increase in absolute exit angle  $\beta_4$ . Both of these effects are noted from the data plotted in figures 7(c) and 7(f) where the tangential component of exit Mach number  $M_{\theta,4}$  increases from 0.83 to 0.91 and the absolute exit angle  $\beta_4$  increases from  $27^\circ$  to about  $37^\circ$  as the shock is moved into the compressor rotor. This increase in change in tangential velocity over the rotor results in an increase in the energy input; thus the compressor rotor operating under these conditions is capable of increased total-pressure ratio.

As the throttle is closed further, the compression shock is moved progressively forward and the total-pressure ratio is again raised until at stall the total-pressure ratio is very near that obtained at wide-open throttle. This increase in total-pressure ratio is accompanied by a decrease in relative Mach number  $M'_4$ , from about 1.30 when the shock in rotor configuration was first obtained to about 0.7, and an increase in discharge angle  $\beta_4$  from  $37^\circ$  to a value of  $56^\circ$ . Over this range of

operation (B-C) there is an increase in adiabatic efficiency from about 0.62 to about 0.68 (fig. 7(g)). This increase in adiabatic efficiency results from the increased useful energy input to the gas without a correspondingly great increase in the absolute losses as the compression shock is moved forward in the compressor rotor.

Static-pressure distribution on outer wall at several back pressures at 104 percent of design speed. - The changes shown for various total-pressure ratios in figure 7 were explained as the result of a compression shock moving into the annulus downstream of the rotor and into the rotor itself as the back pressure is applied. These changes can also be traced in the variations in static pressure along the outer housing. In figure 9, static-pressure distribution for five back-pressure points is plotted over the tip of the compressor rotor and over the annulus downstream of the rotor. Each of these static-pressure distributions can be located on figure 7 by the total-pressure ratio and the downstream Mach number.

For design operation (fig. 9), some acceleration is measured by a decrease in static pressure to a static-to-total pressure ratio of about 0.42 over the first  $2\frac{1}{2}$  inches of the rotor housing. From  $2\frac{1}{2}$  inches to the trailing edge of the rotor (about  $3\frac{1}{2}$  in. at the tip), a sharp rise occurs in static pressure. For design impulse operation, the static pressure at station 5 seems to be about the same as that at the inlet to the compressor rotor. There is a variation in static pressure at station 5 similar to the fluctuation in the annulus between the compressor rotor and station 5. Thus, a part of the fluctuation in the annulus may be due to circumferential location of the static-pressure taps. The other static-pressure distributions shown in figure 9 are for other conditions of back pressure on the compressor rotor and indicate the location of compression shock similar to that described in figure 7.

Performance of compressor rotor at speeds below design. - The performance of this rotor over the range of speeds covered in this investigation is shown in figure 10. Downstream absolute Mach number, adiabatic efficiency, and absolute exit angle are plotted against downstream total-pressure ratio. The data for 104 percent of design equivalent speed are plotted in figure 10 for comparison with the lower-speed data.

At 97 percent of design equivalent speed, operation is very similar to that obtained at design equivalent speed. The total-pressure ratio obtained with shock-in-rotor operation resulted in a higher pressure ratio than impulse-type operation. At the peak total-pressure ratio of impulse-type operation, the absolute exit Mach number at station 4 reached a value of 1.64 (not shown), whereas the highest Mach number measured at station 5 was about 1.45 (fig. 10). Thus, it seems that at 97 percent of design equivalent speed the static pressure could not be reduced sufficiently to move the compression shock completely beyond station 5.

At 91 percent of design equivalent speed, no reversal take place in the trend of total-pressure ratio. The curves for this speed seem to be only that portion of the performance obtained (at higher speeds) for the shock-in-rotor configuration. Thus, at 91 percent of design equivalent speed, the static pressure downstream of the wheel could not be lowered sufficiently to move the shock out of the rotor.

At both the low and the high speeds covered in this investigation, the downstream absolute Mach number and the adiabatic efficiency are the highest at the open-throttle point, whereas the absolute exit angle is at its lowest value. Maximum weight flow also occurs at this condition (fig. 6). As the throttle is closed at these speeds (55, 69, and 83 percent of design equivalent speed), there is very little change in total-pressure ratio but a rather large change does occur in air equivalent weight flow (fig. 6), downstream Mach number, absolute exit angle, and adiabatic efficiency (fig. 10). These changes in performance apparently are a result of the change in wave pattern at the leading edge of the compressor rotor.

Exit conditions as measured by survey data at 104 percent of design equivalent speed; impulse-type operation. - In figure 11, the absolute exit angle is plotted against radius ratio  $r/r_{t,3}$ . Near the center of the passage the absolute exit angle is a minimum value of about  $27.5^\circ$  and is very close to the design value. The measured angle rises to about  $37^\circ$  near the inner wall and about  $33^\circ$  near the outer wall. Near both the inner and outer walls, the measured exit angle is about  $7.5^\circ$  above the design value.

The absolute exit Mach number directly downstream of the rotor at station 4 is shown in figure 11. In the center of the annulus, the absolute exit Mach number is about 1.8 but decreases to about 1.5 near the inner wall and to about 1.4 near the outer wall.

#### DISCUSSION OF RESULTS

Some errors may exist in these measurements because no calibration has been obtained of the immersion effect on the cone type probe at high Mach numbers.

Operational considerations. - The results of this investigation indicate that at design operational conditions this impulse-type supersonic-compressor rotor produced rather uniform exit conditions that are near the design values of exit absolute Mach number and absolute exit angle. However, as the back pressure is built up near the compressor rotor the performance changes considerably. Thus in any application where the rotor is designed to operate with stators as a complete impulse-type supersonic compressor, special attention must be given so that the diffusion is obtained downstream without affecting the rotor.

At the lower speeds of this investigation (55, 69, and 83 percent of design equivalent speed) a wide range of air equivalent weight flow

was obtained. However, as the speed is increased the relative Mach number becomes high and a range of air equivalent weight flows is no longer obtained at 91 percent of design equivalent speed and above. When the relative Mach number is high enough to produce essentially shock-free flow throughout the rotor passage, the compressor makes the transition to impulse-type operation; under this condition the compression shock can be moved in or downstream of the rotor by varying the back pressure. In this investigation, impulse-type operation was obtained at 97 percent of design equivalent speed and above.

Stator requirements for this impulse-type supersonic compressor. - For design operation of the rotor, the inlet Mach number to the stator would be about 1.75 and the flow angle would be about  $27^\circ$ . If the entrance Mach number is reduced by the Kantrowitz contraction ratio, these stators would have an ideal shock recovery of about 0.93. Under these conditions a maximum stage efficiency of 0.75 and stage total-pressure ratio of 3.37 would result. However, it has been pointed out herein that such a set of stators must not impose a static pressure on the rotor which would keep it from developing maximum performance. In some cases the static pressure build-up could move forward through the boundary layer and affect the performance of the compressor rotor. In this case, boundary-layer removal may be necessary to achieve design operation.

It is interesting to note the effects of stators when the compressor rotor is operated very near the stall point. In this case, the stators operate at a Mach number of about 1.2 and the ideal total-pressure recovery is about 0.99. Because the flow angle entering the stators is about  $59^\circ$  from the axial direction and is changing very rapidly, some difficulty may be encountered in stators designed to operate under these adverse air-flow angle conditions.

If the rotor is to operate at design conditions (no shock in the rotor), the stators must not impose a high back pressure on the rotor. At lower than design speeds, fixed stators will limit the mass flow of the compressor, force the rotor to operate with a shock in the rotor passage, and cause a large absolute flow angle at the stator entrance. Solution of these stator problems will require experimental investigation.

Extending performance of impulse-type supersonic-compressor rotor. - Increased total-pressure ratios can be obtained by increasing the supersonic turning in the compressor rotor. This turning, however, results in increased exit angles, Mach numbers, and therefore possibly greater stator losses.

The air equivalent weight flow of this compressor rotor at 104 percent of design equivalent speed was about 29.1 pounds per second. This equivalent weight flow results in a unit weight flow of about 21.0 pounds

per second per square foot of frontal area. In most applications, increasing the unit weight flow above this value would be desirable. Because the axial entrance Mach number is already high, practically all the increased mass flow must be obtained by decreasing the hub-tip ratio. If the rotor-hub diameter is substantially decreased, the lower-hub-section rotational velocity requires increased passage turning if the work input at the hub and tip sections are to be made comparable; a rather wide variation in exit angles therefore results between the tip and hub sections. The three-dimensional effects encountered with large reductions in hub-tip ratio do not seem insurmountable; however, some compromises must be made to obtain the proper balance between variation in exit angles and work input at the hub and tip sections.

The measured adiabatic efficiency of this rotor at design speed was 0.80 at design conditions. In reference 5, a passage with  $90^\circ$  turning resulted in a total-pressure recovery of 0.91 when investigated in cascade. In this cascade investigation, over half of the losses were attributed to mixing losses near the trailing edge of the blades or in the passage directly behind the blading. Thus, a large portion of these losses in the compressor rotor can probably be attributed to mixing losses downstream of the rotor which may be affected by the location of stators in the passage downstream of the rotor.

#### SUMMARY OF RESULTS

The following results were obtained in the investigation of a 16-inch impulse-type supersonic-compressor rotor:

1. This impulse-type supersonic-compressor rotor achieved design operation with essentially shock-free flow through the compressor and the annulus downstream of the compressor rotor.
2. No sharp breaks in performance were obtained from open throttle to stall at any speed.
3. At design conditions, this rotor obtained a total-pressure ratio of about 3.6 at an adiabatic efficiency of 0.80 and an air equivalent weight flow of 29.1 pounds per second.
4. Measured exit Mach number (about 1.72) and flow angle (about  $27^\circ$ ) at the design operational speed were very close to the design values.
5. Stators to be used downstream of this rotor must obtain the required diffusion without imposing a high back pressure on the compressor rotor in order to permit impulse-type operation.

6. High back pressure on the rotor resulted in shock-in-rotor performance. The maximum back-pressure condition at design speed resulted in a total-pressure ratio of about 3.6, and an adiabatic efficiency of 0.66 without changing the air equivalent weight flow. The absolute exit Mach number was about 1.2 for high absolute flow angles.

7. At design speed the weight flow was independent of back pressure, but at the lower speeds a very large range of air equivalent weight flows was obtained with little change in total-pressure ratio.

Lewis Flight Propulsion Laboratory  
National Advisory Committee for Aeronautics  
Cleveland, Ohio

## APPENDIX A

## SYMBOLS

The following symbols are used in this report:

|          |  |
|----------|--|
| A        | area, sq ft  |
| a        | local velocity of sound, ft/sec  |
| D        | diameter, ft   |
| K        | flow coefficient, dimensionless  |
| M        | absolute Mach number, ratio of absolute fluid velocity to local velocity of sound          |
| M'       | relative Mach number, ratio of fluid velocity relative to rotor to local velocity of sound |
| m        | mass flow, slugs/sec   |
| n        | rotor speed, rps   |
| P        | absolute total, or stagnation, pressure, lb/sq ft  |
| p        | static, or stream, pressure, lb/sq ft  |
| r        | compressor radius, ft  |
| T        | absolute total, or stagnation, temperature, °R   |
| t        | static, or stream, temperature, °R   |
| U        | velocity of rotor ( $2\pi rn$ ) at radius $r$ , ft/sec                                     |
| V        | absolute velocity of fluid, ft/sec   |
| W        | weight flow, lb/sec  |
| z        | distance along axis, ft  |
| $\beta$  | angle between compressor axis and absolute fluid direction, deg                            |
| $\gamma$ | ratio of specific heats, dimensionless   |
| $\delta$ | ratio of actual inlet total pressure to standard sea-level pressure, $P_1/2116$            |

2247

$\eta_{ad}$  adiabatic efficiency

$\theta$  ratio of actual inlet stagnation temperature to standard sea-level temperature,  $T_1/518.4$

$\rho$  density, slugs/cu ft

$\phi$  expansion factor, dimensionless

## Subscripts:

1 entrance tank upstream of nozzle

2 downstream of nozzle

3 rotor entrance

4 rotor exit

5 downstream instrument station

a air

f Freon-12

m measured

t tip

z axial component

$\theta$  tangential component

## APPENDIX B

## COMPUTATION OF GENERAL COMPRESSOR DATA

The computation methods described in reference 6 were used for these data. The following changes and additions were required when operating in Freon-12.

Compressor rotor speed in Freon-12. - As recommended in reference 7, design speed was computed in Freon-12 to obtain the design relative Mach number at the compressor-rotor entrance. The design tip-vector diagram for air and the computed tip-vector diagram for operation in Freon-12 at an absolute temperature of 518.4° R are presented in figure 12. Because of guide-vane turning, it is impossible to match exactly the relative Mach numbers at other radii. Thus, it is seen from figure 12 that the design equivalent speed  $U_t/\sqrt{\theta}$  in Freon-12 is 722 feet per second as compared with 1604 feet per second in air. All speeds are given as percent of design speed in Freon-12.

Weight flow. - The entrance nozzle used to obtain the weight flow was calibrated by drawing air through both the nozzle and a calibrated adjustable orifice. The weight flow of Freon-12 was then calculated by use of this calibration and the standard nozzle equations (reference 8)

$$W = 45.50 A_2 K \phi \sqrt{\rho_1 \Delta P}$$

where  $\phi$  for the nozzle was obtained from the following equation:

$$\phi = \left[ \frac{\frac{\gamma}{\gamma - 1} \left( \frac{P_2}{P_1} \right)^{\frac{2}{\gamma}}}{1 - (P_2/P_1)} \frac{1 - (P_2/P_1)^{\frac{\gamma - 1}{\gamma}}}{1 - P_2/P_1} \right]^{\frac{1}{2}} \left[ \frac{1 - (D_2/D_1)^4}{1 - \left( \frac{D_2}{D_1} \right)^4 \left( \frac{P_2}{P_1} \right)^{\frac{2}{\gamma}}} \right]^{\frac{1}{2}}$$

The flow coefficient  $K$  was obtained in the air calibration for  $\gamma = 1.4$  from the known weight flow and the preceding equations. The expansion factor  $\phi$  was then computed by using an assumed average value of  $\gamma$  (1.125) for Freon-12. Then by using the value of  $K$  determined in air, the Freon-12 weight flow was obtained from the original equation for  $W$ .

It was then necessary to determine the approximate air equivalent weight flow from the Freon-12 data. The mass flow through the entrance annulus is given by  $m = \rho VA$ . Then the ratio of mass flow in air to that in Freon-12 is

$$\frac{m_a}{m_f} = \frac{\rho_a V_a}{\rho_f V_f}$$

because A is fixed by entrance geometry.

By substituting for the velocities

$$M = \frac{V}{a}$$

$$\frac{m_a}{m_f} = \frac{\rho_a M_a a_a}{\rho_f M_f a_f}$$

Because conditions of the tests are so set that the axial Mach number is approximately the same in Freon-12 as in air (fig. 12),  $M_a \approx M_f$ .

$$\frac{m_a}{m_f} \approx \frac{\rho_a a_a}{\rho_f a_f}$$

where  $\rho_a$  and  $a_a$  are computed from the usual thermodynamic equations and  $\rho_f$  and  $a_f$  were computed by van der Waals' equations as given in reference 9. The ratio of  $m_a/m_f$  is evaluated from the foregoing equation at the stream Mach number upstream of the entrance guide vanes as determined in the Freon-12 investigation. Then for equivalent weight flows

$$\left( \frac{W \sqrt{\theta}}{a} \right)_a \approx \left( \frac{W \sqrt{\theta}}{\delta} \right)_f \frac{m_a}{m_f}$$

A small error is involved in using  $\theta$  and  $\delta$  to reduce weight flow and speed to standard conditions in Freon-12, which is not a perfect gas.

Adiabatic efficiency and total-pressure ratio are reported as measured in Freon-12.

Pressure and temperature corrections. - Because over a portion of the tests the velocity at the instrument station is supersonic, a correction must be applied to the readings. Total pressure in the supersonic stream was obtained by the simultaneous solution of the equation for the loss over a normal shock

$$\frac{P}{P_m} = \left( \frac{2\gamma}{\gamma+1} M^2 - \frac{\gamma-1}{\gamma+1} \right)^{\frac{1}{\gamma-1}} \left( \frac{(\gamma-1) M^2 + 2}{(\gamma+1) M^2} \right)^{\frac{\gamma}{\gamma-1}}$$

and the ratio of total to static pressure (where the static pressure was measured by the wall taps)

$$\frac{P}{p} = \left( 1 + \frac{\gamma-1}{2} M^2 \right)^{\frac{\gamma}{\gamma-1}}$$

for Freon-12. Because the value of  $P/p$  is relatively insensitive to  $\gamma$ , a mean constant value of  $\gamma$  was used ( $\gamma = 1.125$ ). Static-pressure measurements on the survey probe were obtained by calibration in a supersonic stream.

The relation between total and stream temperature

$$\frac{T}{T} = 1 + \frac{\gamma-1}{2} M^2$$

is very sensitive to  $\gamma$ . In order to obtain stream temperatures a mean  $\gamma$  (1.125) was used for this equation. With the stream temperature thus computed a corrected  $\gamma$  was obtained and was used for a second approximation of the stream temperature.

The values of  $\gamma$  and velocity of sound used in these calculations were obtained from the equations given in reference 9.

The Mach number downstream of the rotor was obtained by using the average total pressure, measured by the total-pressure rakes, and the average wall static pressure. The Mach number was used with the flow angle, measured at the mean radius, to determine the flow components and the relative conditions at station 4.

Adiabatic efficiency. - The total conditions at entrance and exit were used to determine the enthalpy rise for a constant entropy process and for the actual process by the thermodynamic tables of reference 10. The ratio of enthalpy rise under these two conditions was used as the adiabatic efficiency. On several occasions, the adiabatic efficiency was calculated by using the efficiency equation and an assumed constant  $\gamma$ . The adiabatic efficiency obtained in this manner was about two points greater than that obtained from the thermodynamic tables.

## REFERENCES

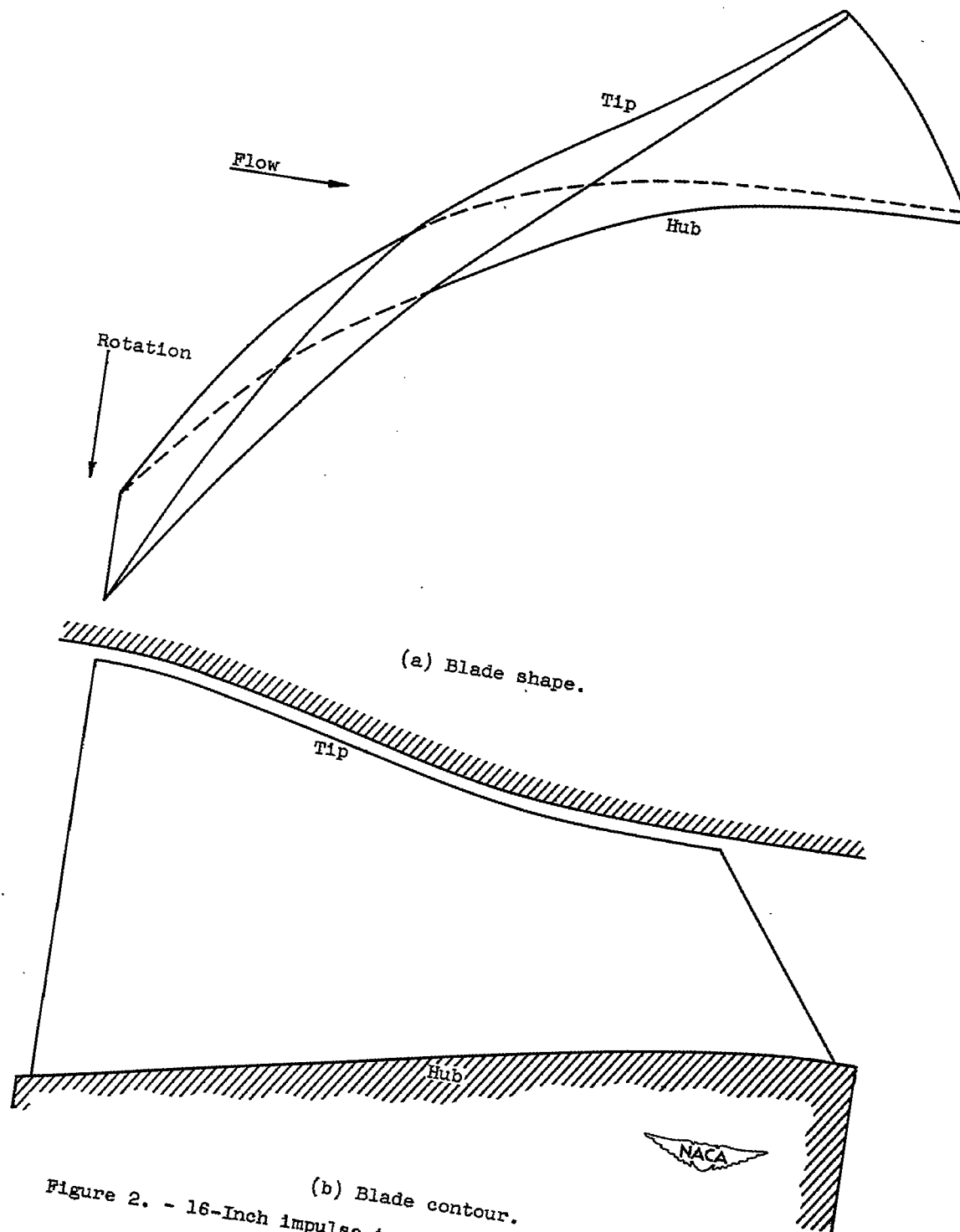
1. Kantrowitz, Arthur: The Supersonic Axial-Flow Compressor. NACA Rep. 974, 1950. (Formerly NACA ACR L6D02.)
2. Wright, Linwood C., and Klapproth, John F.: Performance of Supersonic Axial-Flow Compressors Based on One-Dimensional Analysis. NACA RM E8L10, 1949.
3. Ferri, Antoni: Preliminary Analysis of Axial-Flow Compressors Having Supersonic Velocity at the Entrance of the Stator. NACA RM L9G06, 1949.
4. NACA Subcommittee on Compressors: Standard Procedures for Rating and Testing Multistage Axial-Flow Compressors. NACA TN 1138, 1946.
5. Liccini, Luke L.: Experimental Investigation of the Mixing Loss Behind the Trailing Edge of a Cascade of Three 90° Supersonic Turning Passages. NACA RM L50F21a, 1950.
6. Johnsen, Irving A., Wright, Linwood C., and Hartmann, Melvin J.: Performance of 24-inch Supersonic Axial-Flow Compressor in Air. II - Performance of Compressor Rotor at Equivalent Tip Speeds from 800 to 1765 Feet Per Second. NACA RM E8G01, 1949.
7. Boxer, Emanuel, and Erwin, John R.: Investigation of a Shrouded and an Unshrouded Axial-Flow Supersonic Compressor. NACA RM L50G05, 1950.
8. Anon: Flow Measurement by Means of Standardized Nozzles and Orifice Plates. Ch. 4, pt. 5, A.S.M.E. Power Test Codes, 1940.
9. Huber, Paul W.: Use of Freon-12 as a Fluid for Aerodynamic Testing. NACA TN 1024, 1946.
10. Perry, John H.: Chemical Engineers' Handbook. McGraw-Hill Book Co., Inc., 2d ed., 1941, pp. 2577-2582.



Figure 1. - 16-Inch impulse-type supersonic-compressor rotor.

NACA  
C. 27096

2247



(a) Blade shape.  
(b) Blade contour.  
Figure 2. - 16-Inch impulse-type supersonic-compressor blade.

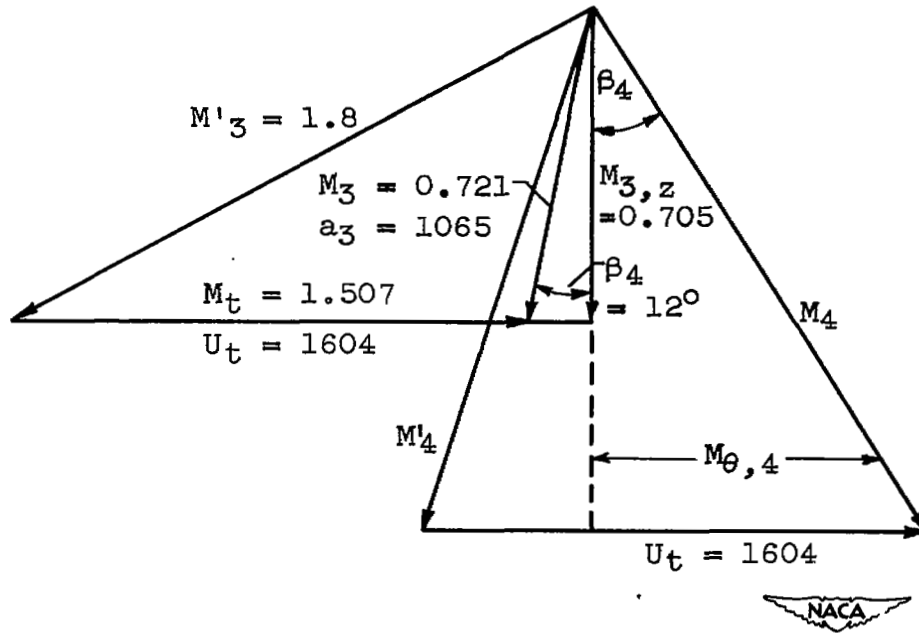


Figure 3. - Design vector diagram for tip section.

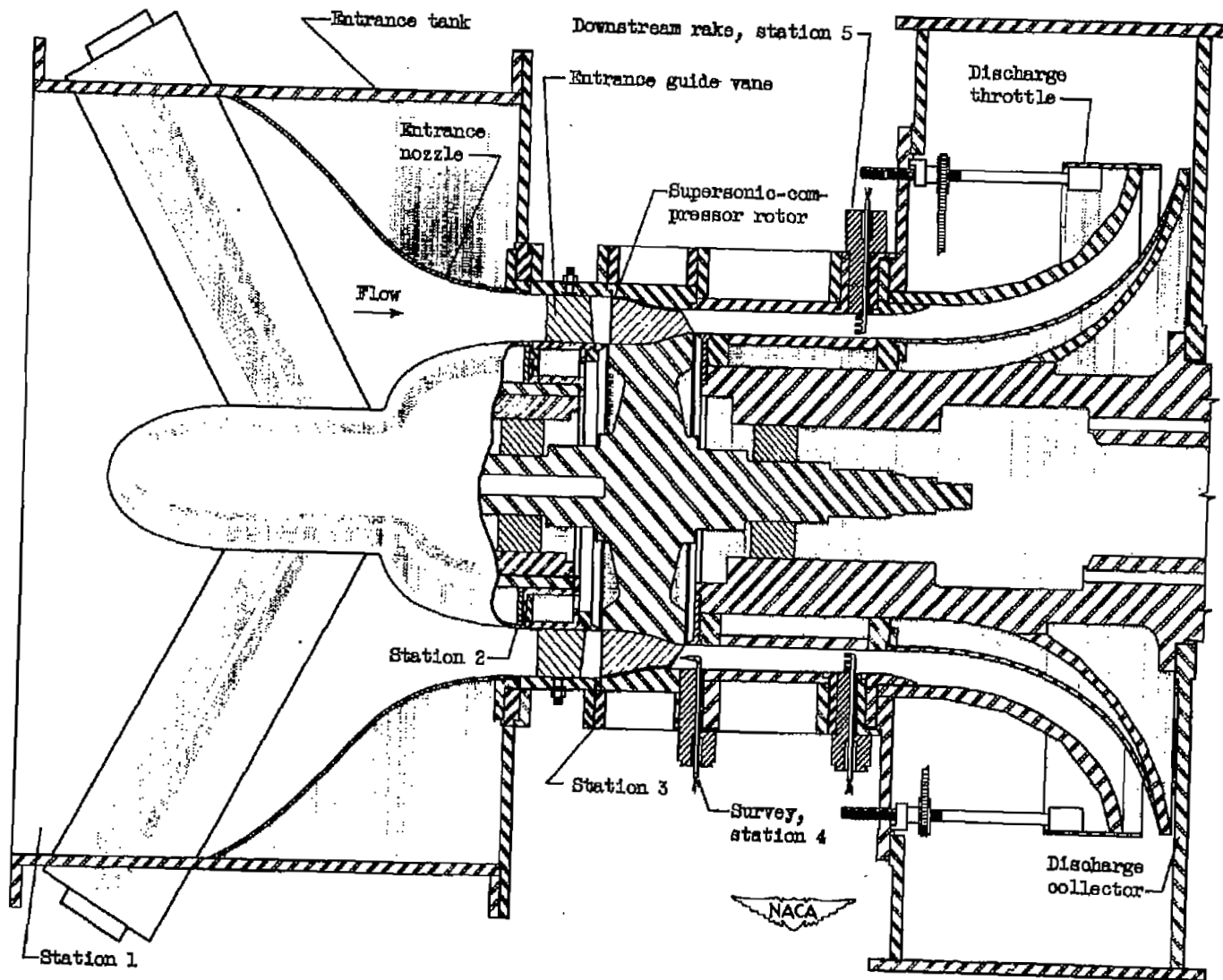
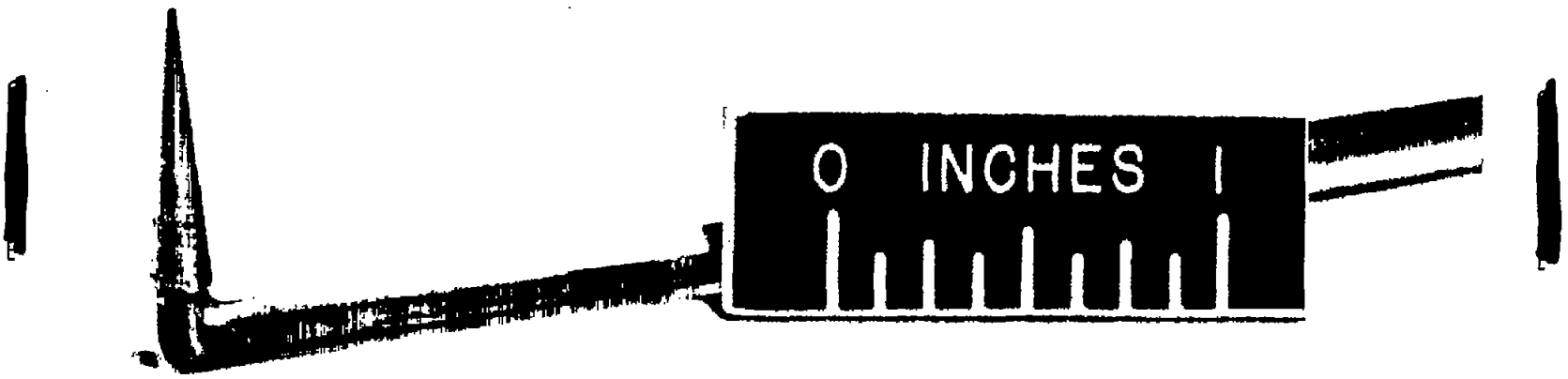


Figure 4. - Schematic diagram of variable-component supersonic-compressor test rig.



NACA  
C-27896

Figure 5. - Cone-type survey instrument calibrated to measure total pressure, static pressure, and flow direction.

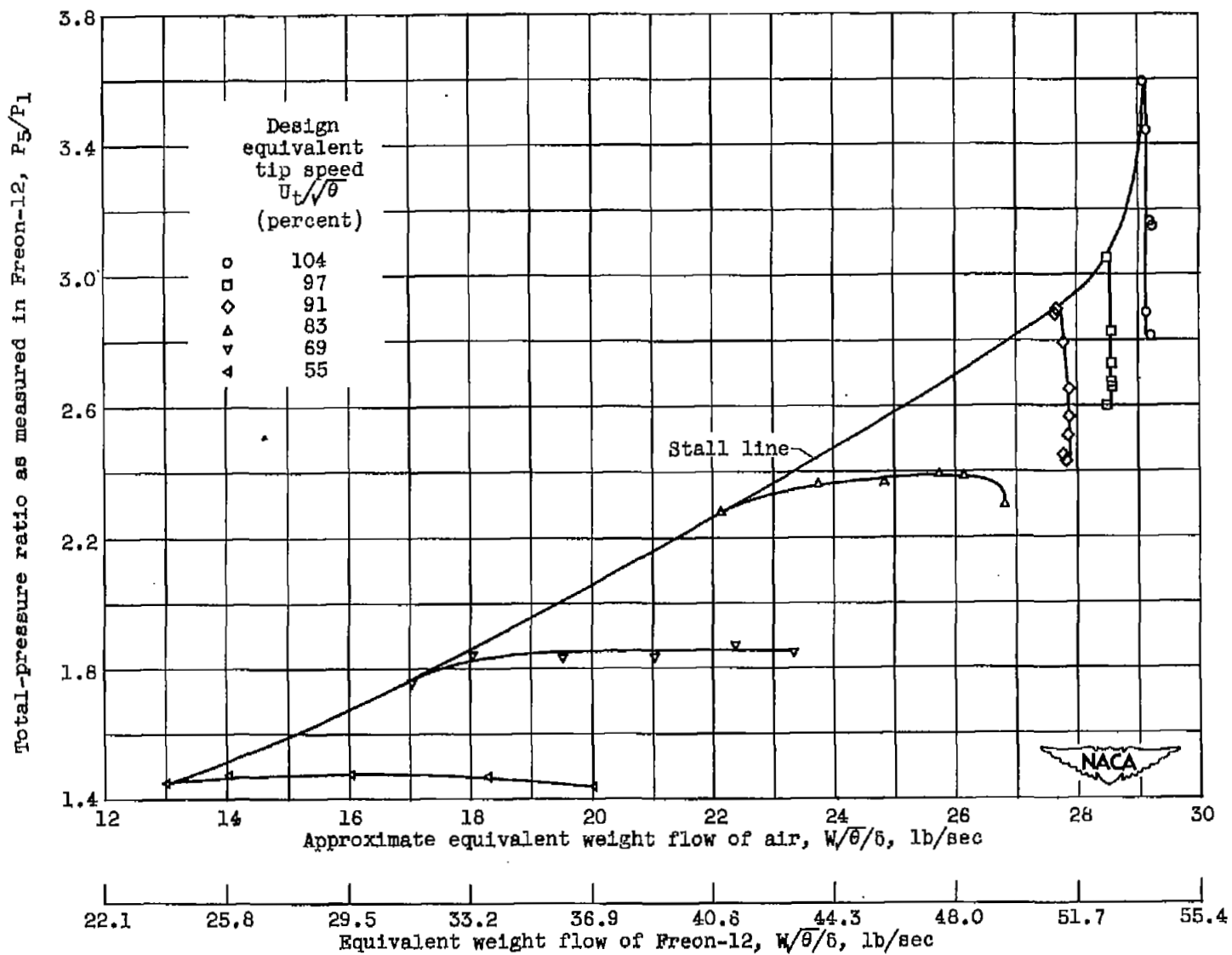


Figure 6. - Performance characteristics for 16-inch impulse-type supersonic-compressor rotor

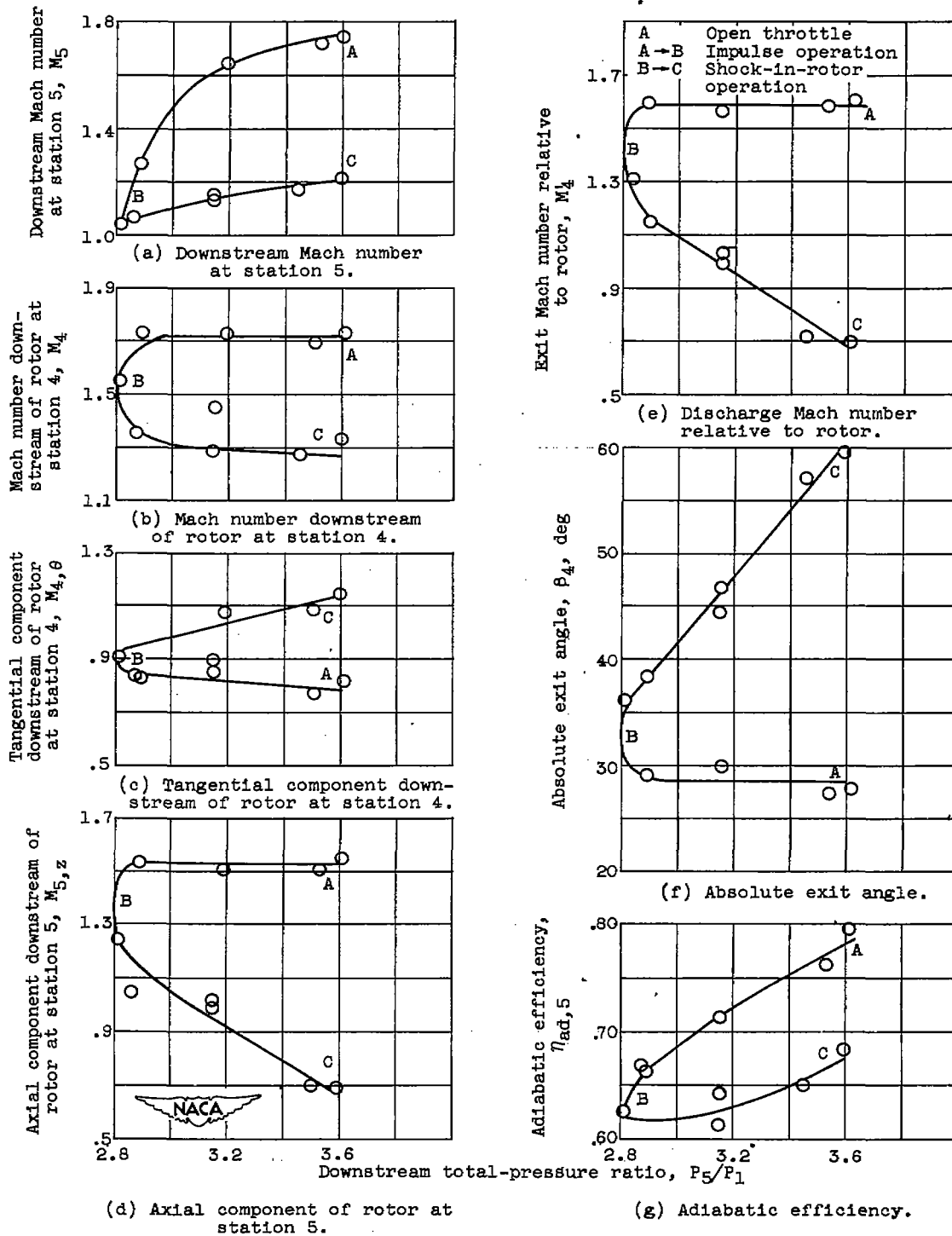


Figure 7. - Conditions downstream of 16-inch impulse-type supersonic-compressor rotor at 104 percent of design equivalent rotor speed as measured in Freon-12.

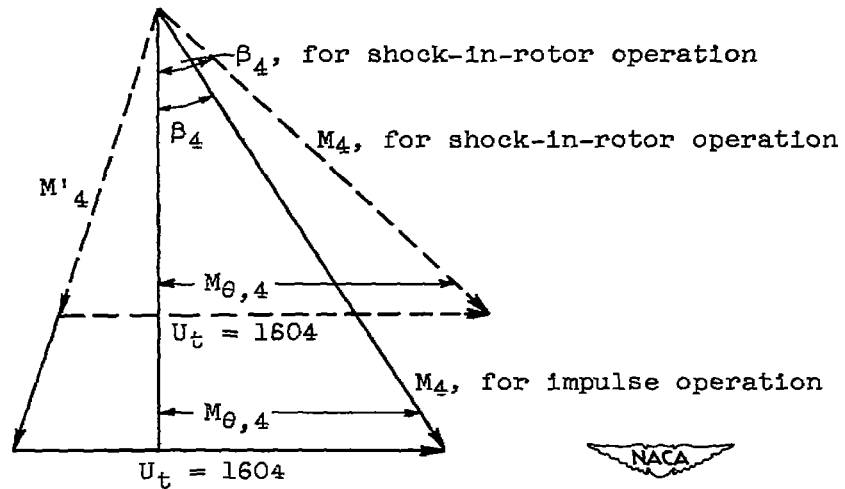


Figure 8. - Vector diagram for impulse-type supersonic-compressor rotor showing effect of moving shock forward into the rotor.

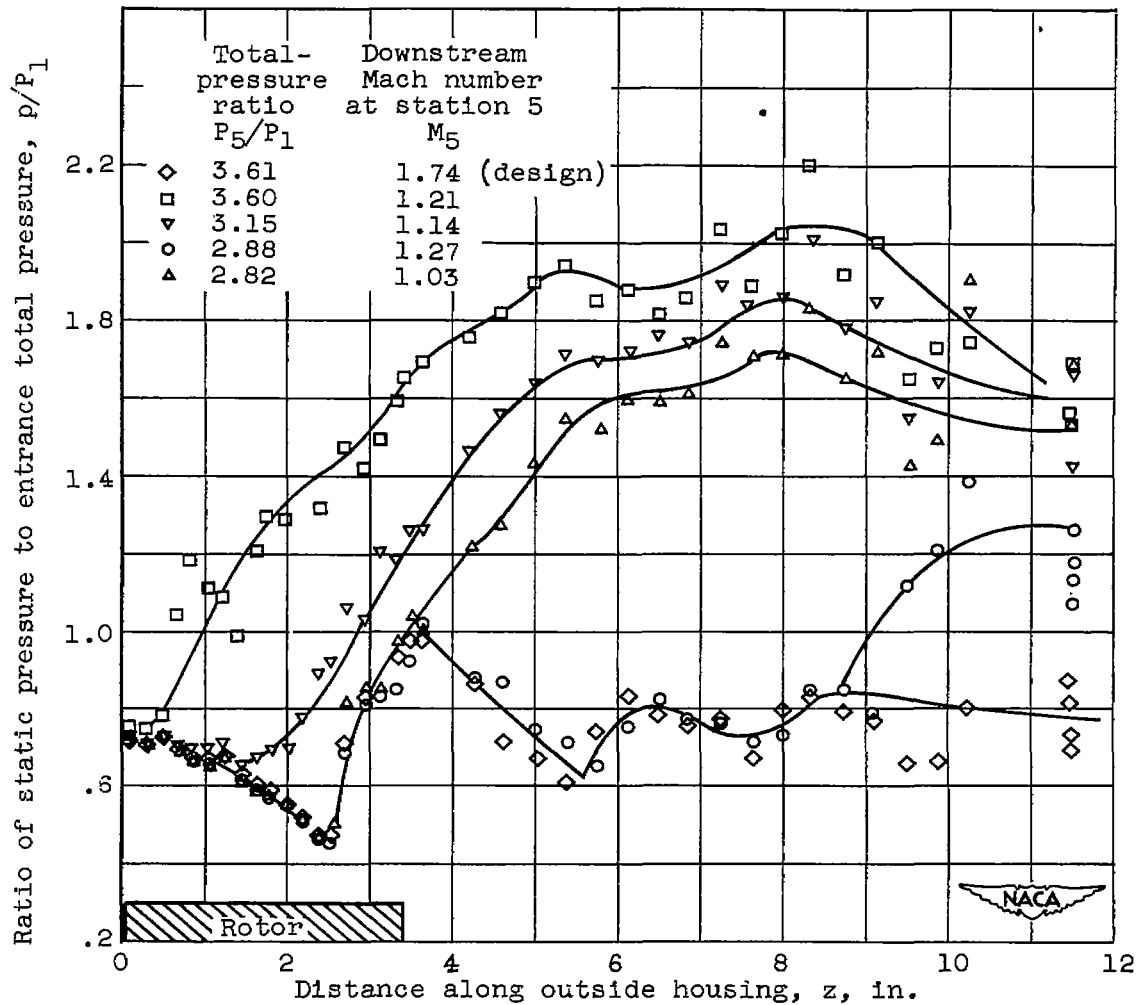


Figure 9. - Static-pressure distributions along outside housing of 16-inch impulse-type supersonic compressor for 104 percent of design equivalent speed and several back pressures.

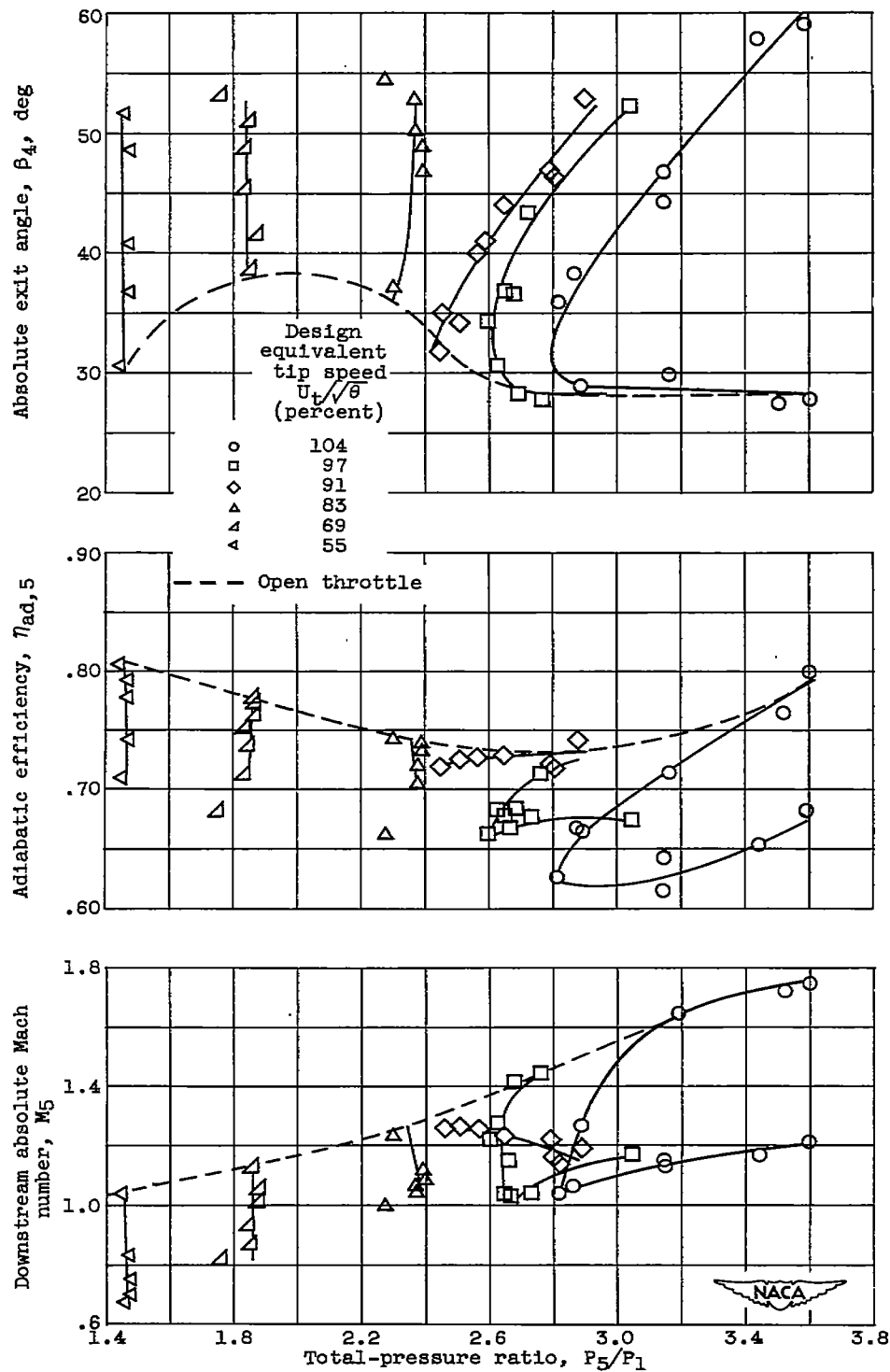


Figure 10. - Performance parameters of 16-inch supersonic-compressor rotor at several compressor-rotor speeds as measured in Freon-12.

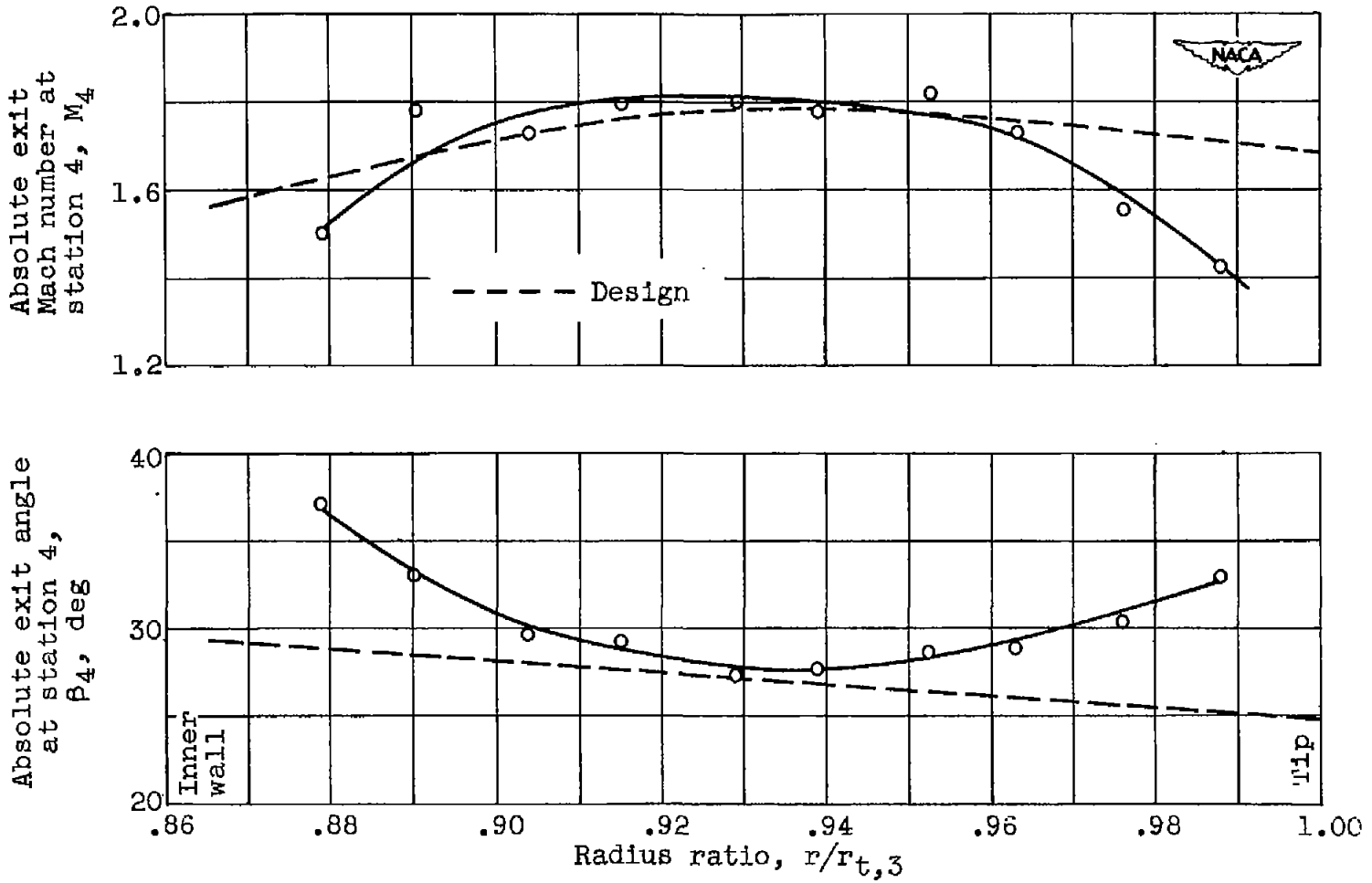
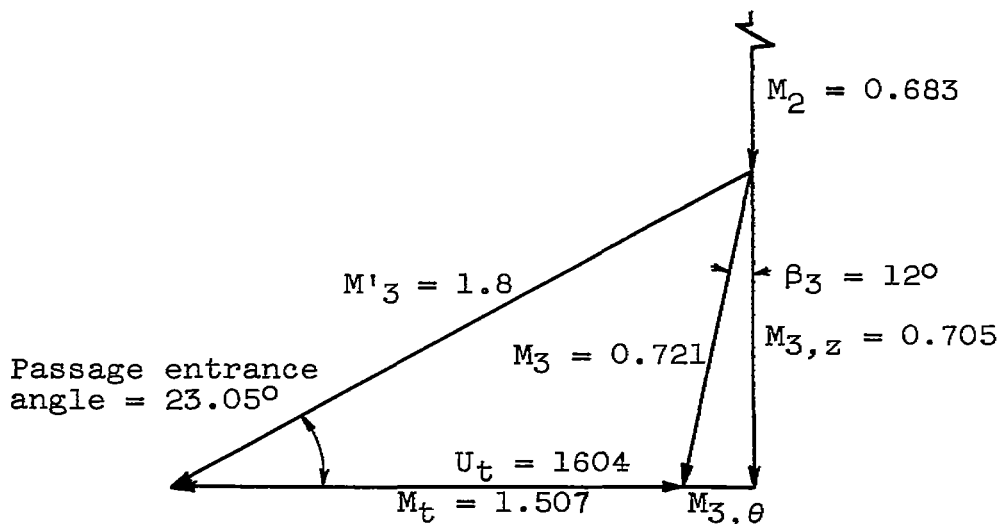
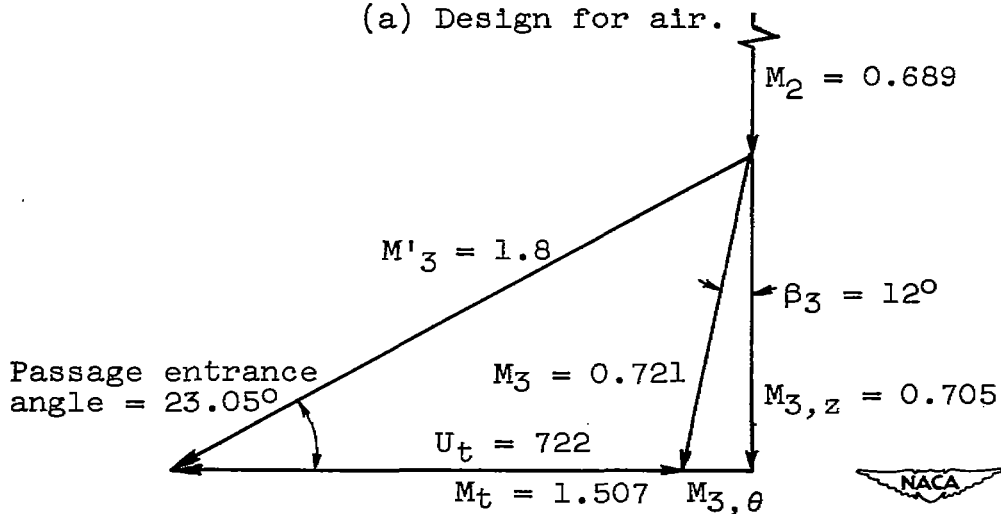


Figure 11. - Survey data obtained over discharge annulus of 16-inch impulse-type supersonic-compressor rotor.



(a) Design for air.



(b) Computed for Freon-12.

Figure 12. - Design entrance tip vector diagram for 16-inch impulse-type supersonic-compressor rotor in air and resulting changes for Freon-12.

NASA Technical Library



3 1176 01435 1374

